A Global Ozone Profile Climatology for Satellite Retrieval Algorithms Based on Aura MLS Measurements and the MERRA-2 GMI Simulation

Jerald R. Ziemke[1,2], Gordon J. Labow[3], Natalya A. Kramarova[1], Richard D. McPeters[1], Pawan K. Bhartia[1], Luke D. Oman[1], Stacey M. Frith[3], David P. Haffner[3]

[1] NASA Goddard Space Flight Center, Greenbelt, Maryland, USA
[2] Morgan State University, Baltimore, Maryland, USA
[3] SSAI, Lanham, Maryland, USA

Abstract. A new atmospheric ozone profile climatology has been constructed by combining daytime ozone profiles from the Aura Microwave Limb Sounder (MLS) and Modern-Era Retrospective Analysis for Research Applications version 2 (MERRA2) Global Modeling Initiative (GMI) model simulation (M2GMI). The MLS and M2GMI ozone profiles are merged between 13 and 17 km (~159 and 88 hPa) with MLS used for stratospheric and GMI for primarily tropospheric levels. The time record for profiles from MLS and GMI is August 2004-December 2016. The derived seasonal climatology consists of monthly zonal-mean ozone profiles in 5-degree latitude bands from 90°S-90°N covering altitudes (in Z* log-pressure altitude) from zero to 80 km in 1 km increments. This climatology can be used as a priori information in satellite ozone retrievals, in atmospheric radiative transfer studies, and as a baseline to compare with other measured or model-simulated ozone. The MLS/GMI seasonal climatology shows a number of improvements compared to previous ozone profile climatologies based on MLS and ozonesonde measurements. These improvements are attributed mostly to continuous daily global coverage of GMI tropospheric ozone compared to sparse regional measurements from sondes. In addition to the seasonal climatology, we also derive an additive climatology to account for inter-annual variability in stratospheric zonal-mean ozone profiles which is based on a rotated empirical orthogonal function (REOF) analysis of Aura MLS ozone

profiles. This REOF climatology starts in 1970 and captures most of the inter-annual variability in global stratospheric ozone including Quasi-Biennial Oscillation (QBO) signatures.

1. Introduction.

McPeters and Labow (2012) (hereafter, ML) and Labow et al. (2015) combined ozone profile data from ozonesondes and the Aura Microwave Limb Sounder (MLS) (Livesey et al., 2011) to use as climatological a priori information for satellite retrievals of ozone. These ozone profile climatologies were constructed by merging ozonesondes in the troposphere with satellite ozone in the stratosphere/mesosphere. For the ML climatology the stratosphere/mesosphere portion of the climatological ozone profiles was based on averaging MLS daytime and nighttime limb measurements. The mix of daytime and nighttime measurements led to smearing of the ozone diurnal cycle in the upper stratosphere and lower mesosphere.

The limited amount and sparse spatial coverage of ozonesonde data has led us to now use the NASA Goddard Earth Observing System (GEOS) Global Modeling Initiative (GMI) model as a substitute for the ozonesonde data in the lower atmosphere. The GMI model uses Modern-Era Retrospective Analysis for Research Applications version 2 (MERRA2) meteorology. We refer to this as the MERRA2 GMI (hereafter M2GMI) model.

We have generated a new ozone profile zonal-mean seasonal climatology (MLS/GMI) based on combining MLS v4.2 and M2GMI ozone profiles which represents an improvement from our previous sonde-satellite ozone climatologies including ML. The earlier climatologies were binned in 10-degree latitude bands due mostly to the limited coverage of sondes. In contrast, the new MLS/GMI ozone profile climatology has been binned to 5^{o} latitude bands by taking advantage of better spatial and temporal coverage of the model output. This new climatology also extends to 80 km in altitude compared to 65 km in the previous climatologies. The new MLS/GMI ozone profile climatology is provided for both volume mixing ratio (units ppmv) and vertical column concentration (Dobson Units (DU) km^{-1}).

We also generated a new inter-annual ozone profile climatology based on MLS ozone, SBUV total ozone, and rawinsonde wind data using a rotated empirical orthogonal function (REOF) method. This REOF inter-annual climatology, just like the MLS/GMI seasonal climatology includes monthly-zonal mean profile ozone concentration (units DU km^{-1}) within 5^o latitude bands and altitudes 0-80 km; however, the REOF climatology represents a long time-dependent record beginning 1970 rather than a 12-month time record for the MLS/GMI climatology.

The application of the MLS/GMI seasonal climatology by itself or together with the REOF inter-annual climatology as a priori enables more accurate profile and column ozone retrievals, including improvements for inter-calibrating and merging independent satellite ozone measurements such as for the SBUV Merged Ozone Dataset (MOD) (Frith et al., 2014). The REOF climatology has recently been used to improve the calibration of long-record ozone measurements from ground Umkehr instruments (I. Petropavlovskikh, personal communication, 2021) and from series of SBUV instruments. The REOF climatology has also recently been used to improve SBUV ozone profile retrievals by adding inter-annual variability which nadir instruments can not retrieve due to a coarse vertical resolution. These SBUV ozone profiles with improved inter-annual variability can be used for the assimilated profile ozone records like one from the Goddard Modeling and Assimilation Office (GMAO)(K. Wargan, personal communication, 2021).

In the following sections we describe the data and GMI model output used in our analysis, outline the methods used to construct the MLS/GMI seasonal climatology and REOF climatology, and discuss the properties of the climatologies. We conclude with a summary of our results. Additional details and figures not covered in the main text are included in a Supplementary Material section.

2. Ozone data and M2GMI model simulated ozone.

2.1. Aura MLS Ozone.

The Microwave Limb Sounder (MLS) instrument onboard the Aura spacecraft makes ozone profile measurements along the orbital track in both daytime and nighttime. Aura is in a sun synchronous orbit, and therefore MLS has nearly complete latitude coverage each day between 82^{o}S and 82^{o}N, with local equatorial crossing times of approximately 1:45 pm for the ascending sunlit portion of the orbit and 1:45 am for the nighttime descending node.

The MLS instrument is a thermal-emission microwave limb sounder that measures vertical profiles of mesospheric, stratospheric, and upper tropospheric temperature, ozone, and several other trace gases from limb scans made ahead of Aura about 7 minutes before the satellite reaches the same point directly below. The MLS instrument primarily uses the 240 GHz microwave band for v4.2 ozone retrievals which for recommended scientific applications extend from 0.0215 hPa to 261 hPa on 38 pressure layers. Vertical spacing for these layers is about 1.3 km everywhere below 1 hPa and about 2.7 km at most altitudes above 1 hPa. By comparison, the vertical resolution for the ozone retrievals is reported to be ~3 km extending from 261 hPa up into the mesosphere. Further details regarding the MLS measurements are described by Livesey et al. (2011). The time record for the MLS ozone used in our study was August 2004 – December 2016. Given the high quality of MLS ozone in the low mesosphere we extend the climatology to 80 km from 65 km where the ML climatology ended. We use only MLS measurements at ascending part of the orbit with a local equatorial crossing time at ~1:45 pm. For most latitudes, that corresponds to the daytime measurements (SZA<90^{o}) from MLS in since the daytime data is most appropriate for many passive UV/Vis ozone remote sensing techniques that require daytime measurements. A number of studies of the diurnal ozone variations in stratospheric and mesospheric ozone [Parrish et al., 2014; Frith et al., 2020, and references therein] demonstrated sizeable diurnal ozone variations around 5-10 hPa.

2.2. SBUV MOD total ozone record.

We use MOD total column ozone measurements from the Solar Backscatter UltraViolet (SBUV) v8.6 retrievals as a proxy to reproduce time-dependent inter-annual variability for the REOF climatology described in Section 4. The MOD total ozone dataset (Frith et al., 2014) is comprised of a composite set of measurements from several SBUV instruments. The first

instrument was Nimbus-4 BUV launched in 1970, followed by the second and improved version SBUV on Nimbus-7 launched in October 1978. Starting in 1989, seven SBUV/2 instruments were launched beginning with NOAA-9, followed by NOAA 11, 14, 16, 17, 18, and 19. Currently this record is extended with the Ozone Mapping and Profiler Suite (OMPS) nadir-profiler (NP) on board the Suomi National Polar-orbiting Partnership (SNPP) satellite. There are four follow-up OMPS instrumental suites as a part of JPSS program (with JPSS-1/NOAA-20 already in operation) that will extend the SBUV-type ozone observations in the next two decades. The SBUV instruments retrieve broad ozone profiles from measurements of backscattered solar UV radiation which can be integrated to give total column ozone. All MOD instrument measurements have been processed using the v8.6 retrieval algorithm as described by McPeters et al. (2013) and Bhartia et al. (2013). In this study we use monthly zonal-mean gridded total ozone extending from 90^{o}S to 90^{o}N at 5^{o} latitudinal binning (Frith, 2021, personal communication). The MOD total ozone record spans from January 1970 to December 2020 with some temporal gaps, including May 1976-October 1978 due to missing Nimbus-4 BUV measurements.

2.3. Ozonesonde measurements.

We include balloon-launched ozonesonde measurements for comparison and validation of the M2GMI simulated tropospheric ozone. The used ozonesonde database extends from 2004-2019 and includes measurements from the Southern Hemisphere ADditional OZonesondes (SHADOZ) program (Thompson et al., 2017; Witte et al., 2017), the World Ozone and Ultraviolet Data Center (WOUDC) (https://woudc.org/), and the Network for the Detection of Atmospheric Composition Change (NDACC). (http://www.ndsc.ncep.noaa.gov/). The ozonesondes provide daily ozone profile concentrations generally a few times per week as a function of altitude; we include ozonesonde data from several dozen global sites. Most of the sonde ozone profile measurements that we use are from Electrochemical Concentration Cell (ECC) instruments. The sonde ozone profiles were integrated vertically each day from surface to tropopause to derive tropospheric column ozone (TCO) measurements using the same tropopause pressures as used for M2GMI TCO. Tropopause pressure for both sonde and GMI

TCO was derived from National Centers for Environmental Prediction (NCEP) re-analyses based on the World Meteorological Organization (WMO) 2K km^{-1} temperature lapse-rate definition.

In section 4 we describe construction of the REOF inter-annual ozone profile climatology that includes monthly tropical Quasi-Biennial Oscillation (QBO) zonal winds. The tropical QBO zonal winds come from the Maldives (January 1970 - December 1975) and Singapore (January 1976 - present) rawinsonde record (Univ. Berlin, https://www.geo.fu-berlin.de/met/).

2.4. MERRA-2 GMI simulated ozone.

The M2GMI simulation is produced with the Goddard Earth Observing System (GEOS) modeling framework (*Molod et al*., 2015), using winds, temperature, and pressure from the MERRA-2 reanalysis (*Gelaro et al*., 2017). The configuration for this study is a dynamically constrained replay (*Orbe et al*., 2017) coupled to the Global Modeling Initiative's (GMI) stratospheric and tropospheric chemical mechanism (*Duncan et al*., 2007; *Oman et al.,* 2013; *Nielsen et al*., 2017). The simulation was run at ~0.5° horizontal resolution, on the cubed sphere, and output on the same 0.625° longitude x 0.5° latitude grid as MERRA-2 from 1980-2016. We refer to Strode et al. (2015, 2020) for details of the M2GMI model simulation. The daily M2GMI ozone profiles were averaged monthly and re-gridded from the original resolution to zonal means in 5° latitude bands; the original 72 layers of the simulated profile ozone were also re-mapped to Z^* altitudes with 1 km vertical spacing (section 3.2).

2.4.1. Evaluation of M2GMI simulated tropospheric ozone.

Ozone profiles generated by the M2GMI simulation have been extensively evaluated in a number of studies. Stauffer et al. (2019) provide a detailed global analysis of M2GMI ozone profiles using comparisons with ozonesondes. On average they found differences of about ±5% between M2GMI and sondes in the troposphere from 38 sonde stations from 69°S-79°N (their Fig. 1). The largest differences were in the tropics where M2GMI was lower than sonde by up to 10-20% in low-mid troposphere, but in the tropical tropopause region M2GMI was higher than sonde by 40-50%; the large percentage differences however can be due to relatively low mean

182 background ozone concentrations of only ~1-2 DU km^{-1}. Wargan et al. (2018) compared the
183 annual mean ozone mixing ratio anomalies for 1998-2016 between sondes and M2GMI at
184 several stations for 70 hPa, 100 hPa, and 200 hPa. Their comparisons show squared correlations
185 varying from 0.62 to 0.93 and they concluded that the M2GMI simulation well captures the
186 variability of tropospheric ozone including the UTLS region. Ziemke et al. (2014) provide
187 additional evaluation of M2GMI tropospheric ozone by comparing with ozonesondes, satellite,
188 and Global Modeling and Assimilation Office (GMAO) data assimilation; the M2GMI and sonde
189 daily comparisons from tropics to high latitudes in both hemispheres (their Figs. 2-7) showed
190 offsets and standard deviations of differences varying ~0-2 DU (~0-7%) and 4-7 DU (~15-23%),
191 respectively. The M2GMI simulated ozone profiles have also been extensively compared with
192 Atmospheric Tomography Mission (ATom) aircraft flight measurements (Bourgeois et al., 2020)
193 for years 2015 and 2016 (Junhua Liu, personal communication, 2020). The ATom in-flight
194 measurements of ozone volume mixing ratio are found to compare closely with M2GMI
195 simulated ozone, generally within about ±20% along each of the mission flight paths that
196 included meandering ascent and descent between near surface and tropopause each day.
197
198 Our study also includes evaluation of M2GMI simulated tropospheric ozone. Figure 1 compares
199 sonde and M2GMI Tropospheric Column Ozone (TCO) where the sonde and M2GMI
200 measurements have been space-time co-located at the sonde station sites and seasonally averaged
201 for 2004-2016. The collocation involved matching daily TCO from the sondes with M2GMI
202 daily TCO at $5^o \times 5^o$ gridded resolution interpolated to each sonde latitude-longitude location. As
203 noted in section 2.3, both daily sonde and M2GMI TCO were derived using the same NCEP
204 WMO tropopause pressures.
205
206 The M2GMI modelled ozone in Fig. 1 closely simulates the sonde measured ozone year-round
207 with an exception in the NH mid-high latitudes in MAM and JJA where the simulation tends to
208 underdetermine sonde TCO by ~5 DU or more. Section S3 of the Supplementary Material
209 includes additional discussion and figures regarding evaluation of M2GMI tropospheric ozone
210 profiles using ozonesondes and surface lidar measurements.
211

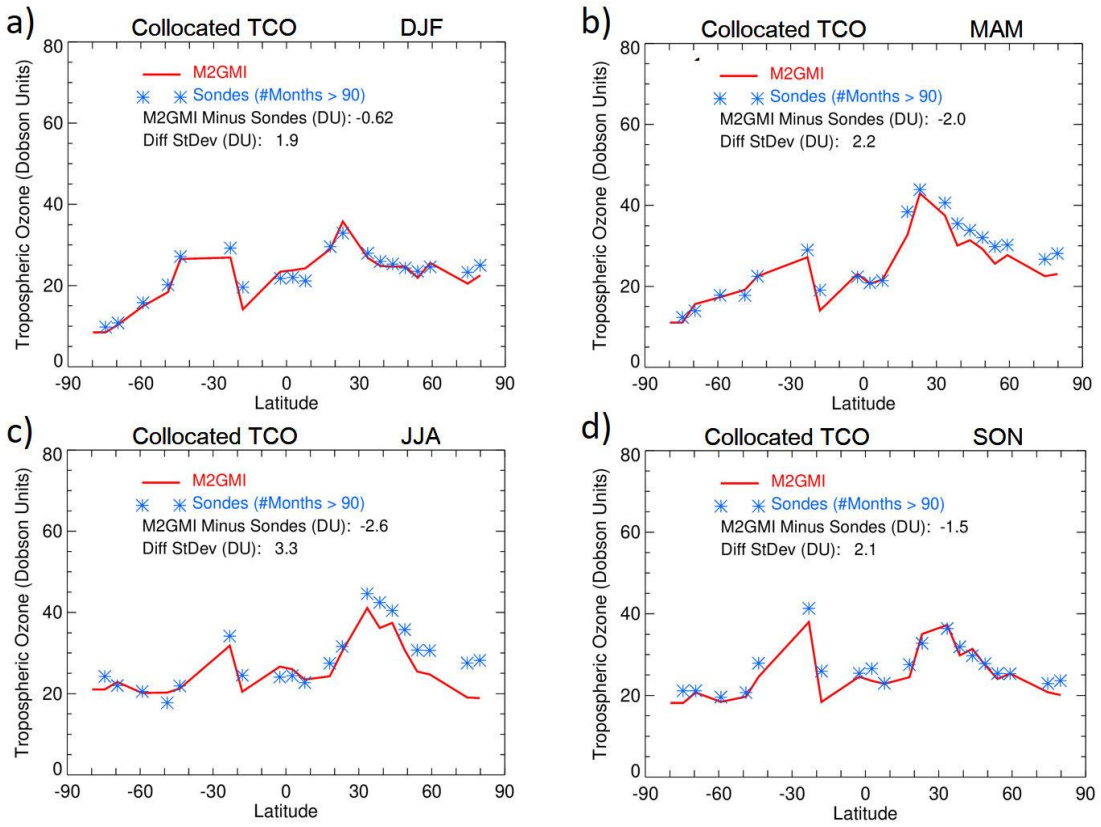

Figure 1. Comparisons between M2GMI simulated (red curves) and ozonesonde TCO (blue asterisks) averaged over three-month seasons (indicated) for 2004-2016. The M2GMI TCO field is sampled daily at the sonde station locations. All TCO is in Dobson Units. The same daily tropopause is used for both M2GMI and sonde to derive TCO, and is defined as according to the WMO 2 K km^{-1} lapse-rate tropopause definition using NCEP temperatures. Included in each panel are mean offsets and standard deviations of TCO seasonal differences.

3. The MLS/GMI seasonal climatology.

The MLS/GMI seasonal climatology product is derived for both volume mixing ratio (units ppmv) and vertical column concentration (DU km^{-1}); the latter has vertical and latitudinal structure that is closely similar to that of ozone number density and ozone partial pressure. Standard deviations are reported for both mixing ratios and column concentrations based upon all available daily ozone profiles over a given month and within every 5° latitude band. The standard deviations provide a measure of climatological ozone variability and are important for

error covariance matrices included as a priori information in retrieval algorithms such as the optimal estimation method of Rodgers (2000). We refer the reader to the Supplementary Materials for further discussion and figures involving calculated standard deviations.

3.1. Global coverage of M2GMI tropospheric ozone compared to sondes.

Our motivation for using M2GMI simulation is that they provide better spatial and temporal representation of tropospheric ozone profiles than ozonesondes. The sondes are sparsely distributed over the Earth with generally only a few measured profiles per month for a given station. The limited spatial coverage of sondes is demonstrated in Fig. 2 with M2GMI mid-tropospheric ozone concentration (ppbv) at height Z^*=5 km for climatological May (Z* is approximately equal to actual altitude and is defined in section 3.2.)

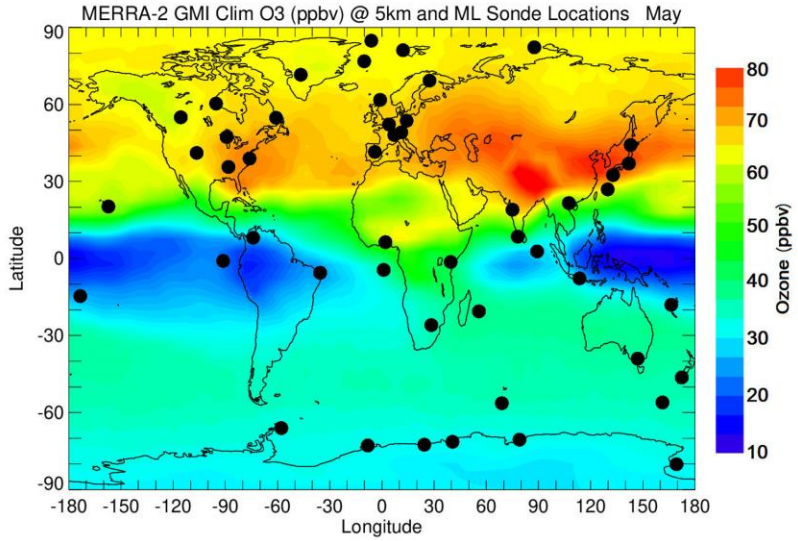

Figure 2. Map of climatological ozone volume mixing ratio (in ppbv) from the M2GMI simulation at Z^*=5 km altitude (see section 3.2) for the month of May. Blue color indicates areas with ozone concentration of about 10 ppbv and red color corresponds to regions with > 75 ppbv. Black circles show locations of the sonde stations with a long observational record. Data from these stations were used to constrain tropospheric ozone profiles in the ML climatology.

Tropospheric ozone exhibits planetary-scale variability that includes a year-round zonal wave-1 pattern in the tropics (greatest amplitude in September-October) and large-scale patterns outside the tropics that vary greatly with season and region (Fishman et al., 1990). The tropical wave-1 in tropospheric ozone originates from regional sources of ozone: lightning, biofuel & biomass burning, stratosphere-troposphere exchange (STE), and transport associated with the tropical east-west Walker circulation. In the extra-tropics, the large planetary scale features in tropospheric ozone have strong seasonal dependence with the seasonal maximum in JJA in the NH and SON in the SH. These seasonal patterns in tropospheric ozone outside the tropics are also due to combined effects from STE, biofuel, lightning, biomass burning, and long-range transport. The global planetary-scale patterns in tropospheric ozone columns were first shown from TOMS/SAGE (Fishman et al., 1990) and TOMS/MLS (Ziemke et al., 1996) satellite measurements. The patterns in the M2GMI tropospheric ozone mixing ratio for Z* = 5 km in Fig. 2 in the tropics and in the NH are similar to the TCO May pattern from satellite records.

It is apparent from Fig. 2 that the ensemble of ozonesondes is unlikely to effectively represent the zonal mean tropospheric ozone values due to their limited sampling. For example, in the tropics the sonde measurements under-sample the tropical wave-1 structure in tropospheric ozone. Due to the under-sampling in the tropical Pacific area, sondes do not capture the very low ozone concentrations of ~10 ppbv. This leads to the over-estimation of zonal-mean tropospheric ozone in the tropics from the sondes. We will show later that this over-determination of ML tropospheric ozone in the tropics averages to about 5-10 DU in TCO year-round between 20^{o}S-20^{o}N. The sondes also tend to miss the high values of ozone in the NH mid-latitudes over the Asian continent (see Fig. 2), thus introducing a low bias in zonal-mean tropospheric ozone in NH mid-latitudes.

3.2. Merging MLS and M2GMI ozone profiles.

Simulated ozone volume mixing ratio values from the M2GMI model were merged with ozone volume mixing ratio measurements from MLS to construct the ozone profile seasonal climatology in the format of monthly zonal means. The merging of MLS and M2GMI ozone involved monthly zonal-mean ozone profiles for both records in 5^o latitude bands with Z*

altitudes 0-80 km (1 km increments). For low and mid-latitudes between 40°N and 40°S the M2GMI and MLS profiles were merged for Z* levels between 13 km and 21 km (156 hPa to 49 hPa). For latitudes poleward of 40° in each hemisphere the profiles were merged slightly lower in the atmosphere, for Z* levels between 8 km and 16 km (320 hPa to 101 hPa). Within the merged altitude ranges the climatology is weighted linearly, from 100% M2GMI at the lowest altitude to 100% MLS at the highest altitude. Standard deviations were calculated for each climatological ozone value.

As in previous climatologies, the altitude variable used for our climatology is Z*, a parameter frequently used in comparisons of atmospheric chemistry models (Park et al., 1999). Z* is in units of kilometers but can be considered a pressure variable. Z^*(km) is defined by $Z^*=16\cdot\log(1013/P)$ where P is atmospheric pressure in units hPa. The altitude spacing for our climatology is 1 km in Z* units. In an isothermal terrestrial atmosphere Z* would correspond closely to altitude.

3.3. Comparisons with the ML Climatology.

We first examine basic global patterns of the MLS/GMI seasonal climatology. Figure 3 shows vertical column concentrations (DU km^{-1}) for the climatology by 3-month season (indicated) for Z* = 0-80 km. Column concentrations in the low stratosphere in both hemispheres are largest during winter-spring and smallest in summer. In both hemispheres, ozone is largest in the winter-spring months due to seasonal transport from the tropics to the extra-tropics in winter-spring months (i.e., the Brewer Dobson Circulation) and longer lifetimes for ozone in the low stratosphere. The highest ozone amounts in Fig. 3 are ~18-20 DU km^{-1} in the NH around 20 km during winter and spring. In the troposphere, very low ozone density of less than 2 DU km^{-1} occurs in the tropics year-round.

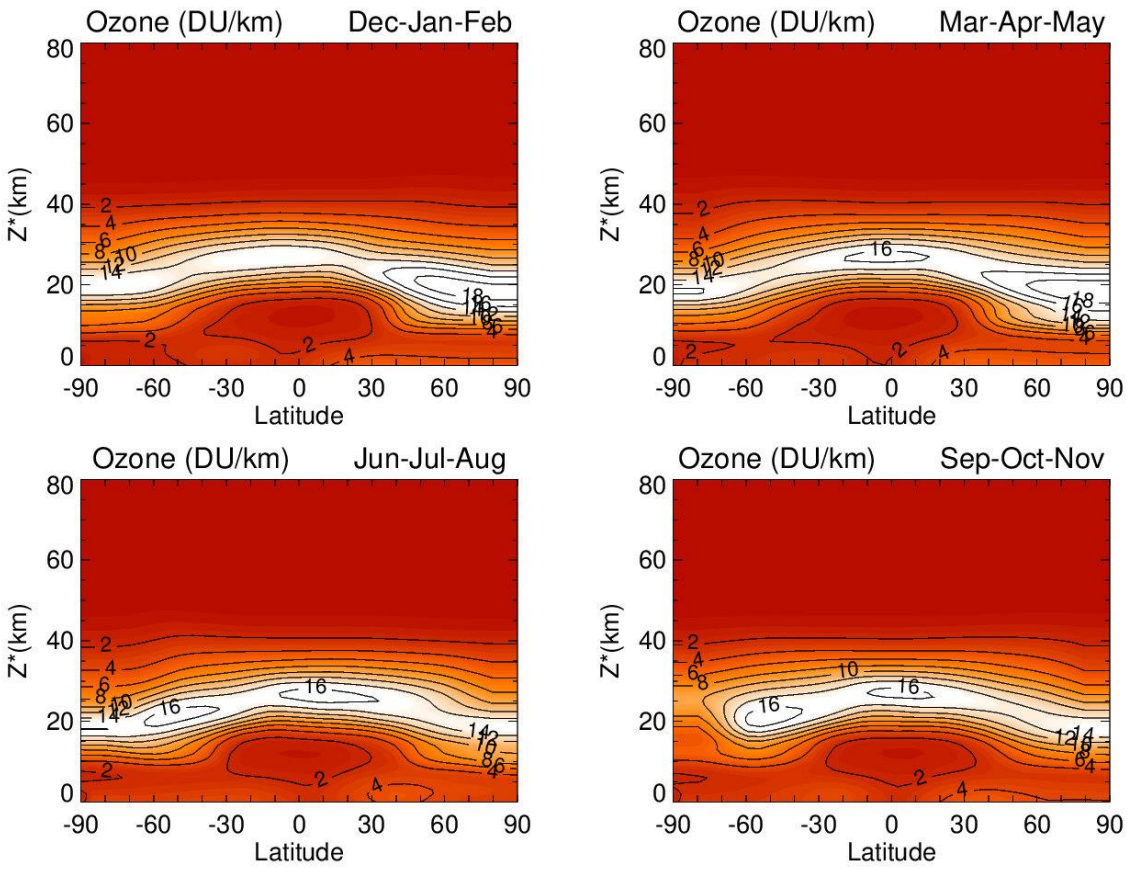

Figure 3. Meridional cross-sections of derived zonal-mean vertical ozone concentration (units DU km^{-1}) for the MLS/GMI seasonal climatology. This 12-month climatology is averaged over three-month seasons (indicated) for 2004-2016 and is binned for 5° latitude bands and Z^* levels from 0-80 km at 1 km spacing (see text).

While the basic characteristics of stratospheric ozone in Fig. 3 are important to note, our main focus is to compare tropospheric ozone in Fig. 3 with the ML sonde ozone climatology. Because the ML climatology uses sparsely sampled sonde measurements to estimate zonal-means in the troposphere, it is possible that there may be substantial differences.

Figure 4 shows the difference between ML and MLS/GMI zonal-mean profile ozone by season, plotted as Z* altitude versus latitude. Only Z^* levels 0-30 km are included in Fig. 4 to highlight differences in ozone profiles used for the troposphere and the low stratosphere merging region. Year-round positive differences in the tropics in Fig. 4 suggest that ML is always too large in the

low-mid troposphere compared to M2GMI due to absence of ML sonde measurements in the Pacific region where tropospheric ozone is low (e.g., Fig. 2). At latitudes around ±35^{o} and elsewhere in the low stratosphere merging region in Fig. 4 there are anomalous differences from −0.5 up to +1.5 DU km^{-1}; these sharp patterns are ascribed to sonde sampling issues for the ML climatology. In the boundary layer throughout the NH extra-tropics during winter (i.e., upper left panel in Fig. 4) the M2GMI ozone is higher than sondes by ~0.5 to 1 DU km^{-1}. These latter differences are attributed to a known model issue related to underestimating surface deposition over cold surfaces (Jaegle et al. 2018), most prominent in the NH boundary layer during winter. When compared with ML in Fig. 4, the model in this region over-determines the ozone column in DJF by about 2 DU.

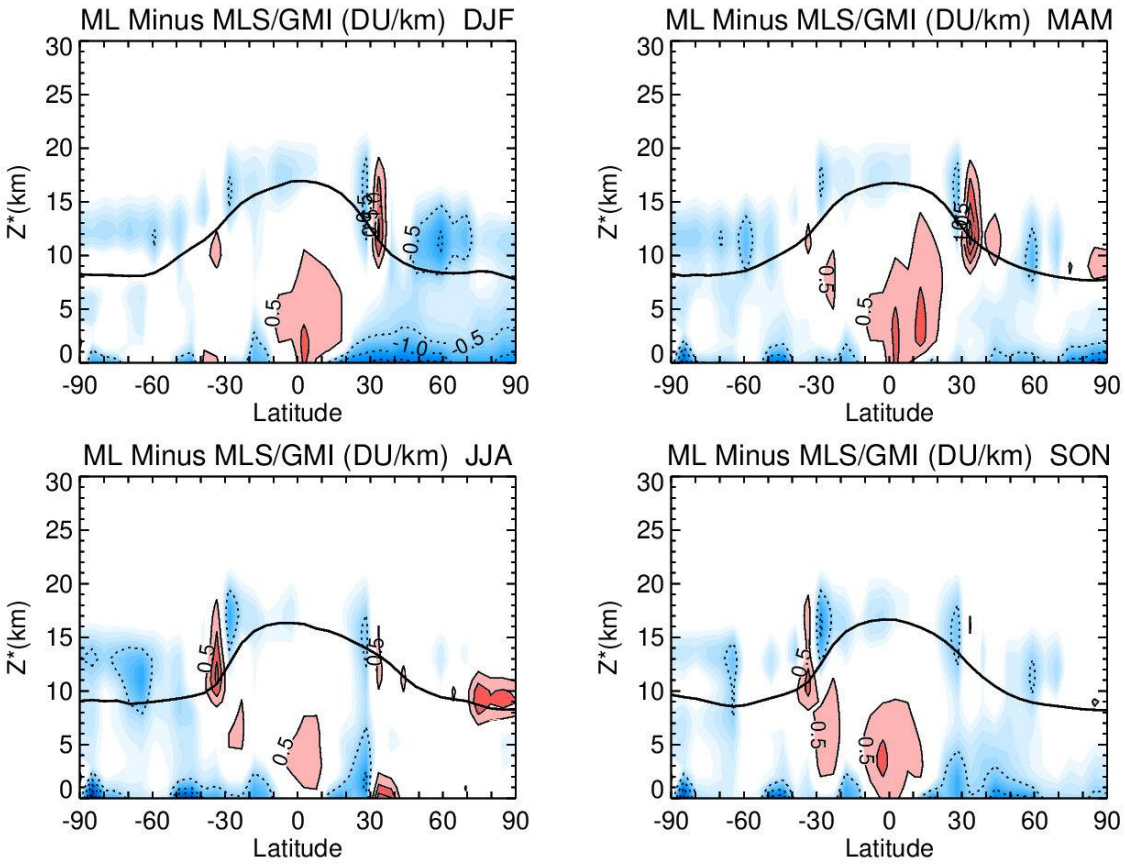

Figure 4. Meridional cross-sections of ML minus MLS/GMI climatologies of ozone column concentration (DU km^{-1}). These differences are averaged over three-month seasons (indicated) for 2004-2016 and are binned for 10^{o} latitude bands and Z* levels from 0-30 km at 1 km spacing.

Contour levels (indicated) increment by 0.5 DU km^{-1} with blue/dashed contours meaning negative, and pink/red solid contours meaning greater than 0.5DU km^{-1}. The black line indicates tropopause height according to the WMO 2 K km^{-1} lapse-rate tropopause definition using NCEP temperatures. White color denotes zero differences.

Line plots of seasonal differences (ML minus MLS/GMI) of integrated ozone columns are shown in Fig. 5 for 0-8 km (Fig. 5a) and 0-16 km (Fig. 5b). These line plots are determined from Fig. 4 by summing the 1 km layers of ML minus MLS/GMI differences. In the tropics 0-16 km integrated column in Fig. 5b represents the total troposphere (i.e., TCO) with ML larger than MLS/GMI by about 10 DU year-round. Comparison with the 0-8 km columns in the left panel show that these differences in the tropics originate mostly from the lower troposphere which is consistent with all four panels in Fig. 4. Outside the tropics in Fig. 5 there are seasonal offset differences in the NH up to -5 to -10 DU during DJF. Part of the reason for the ML minus MLS/GMI biases in Fig. 5 is due to sonde under-sampling for the ML climatology, particularly in the tropics as noted for Fig. 4. The sonde under-sampling also creates the sharp (non-physical) variability seen between adjacent latitude bins in Fig. 5.

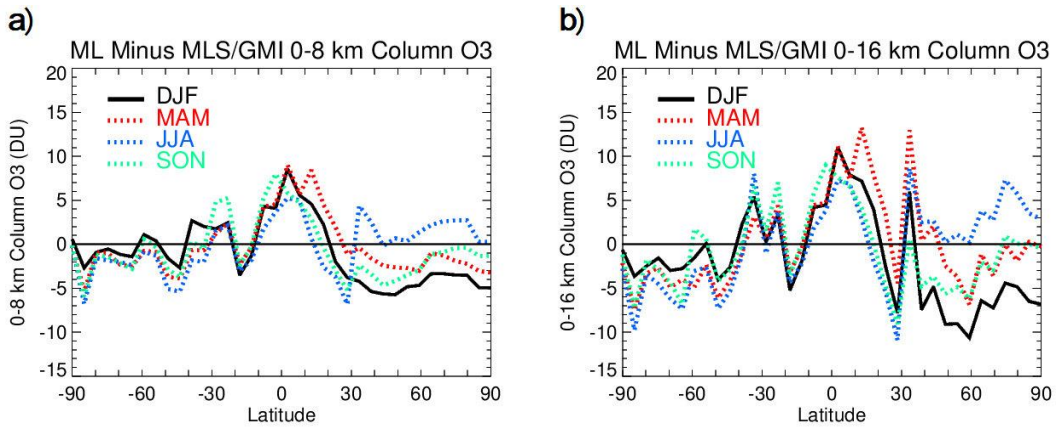

Figure 5. (a) Line plots of seasonal differences of ML minus MLS/GMI integrated ozone columns for 0-8 km. The differences are averaged over three-month seasons (indicated by DJF, MAM, JJA, and SON). (b) Same as (a), but for 0-16 km ozone columns.

4. An inter-annual ozone profile climatology.

The MLS/GMI seasonal climatology captures the vertical shape of zonal-mean ozone profiles by season and latitude in both troposphere and stratosphere. However, inter-annual processes such as the QBO produce sizeable changes in the vertical ozone distribution in stratospheric ozone from year to year. To capture these variations, we have constructed a global time-dependent climatology of stratospheric ozone that represents ozone inter-annual variability. This climatology can be used either independently or added to the MLS/GMI seasonal climatology, depending on the particular application.

The derivation of the inter-annual ozone climatology is lengthy and is discussed in detail in the Supplementary Materials. In this section we provide only a short overview of the methodology and discuss the final product. The inter-annual ozone climatology is constructed using a method that includes an REOF analysis as described by Richman (1986, and references therein). With our approach, vertical information for the climatology comes from an REOF analysis of MLS ozone profiles, while month-to-month time dependence follows by coupling the REOF analysis time coefficients with SBUV MOD total ozone and tropical QBO zonal winds. The time period for the REOF climatology depends on the availability of total ozone and tropical QBO winds. The time period for this climatology is 1970-2018 (588 consecutive months) with gaps present due to some missing MOD total ozone including Nimbus 4 measurements in the 1970s. We plan to periodically extend this REOF climatology when zonal wind and MOD total ozone data become available. Before applying the REOF approach, an Empirical Orthogonal Function (EOF) method (Kutzbach 1967, and references therein) was applied to MLS ozone anomaly profiles to derive repeatable inter-annual patterns in the ozone vertical distribution; that is, the EOF analysis was applied to MLS monthly zonal-mean ozone profile anomalies derived by removing seasonal cycles between August 2004 and December 2016. All MLS ozone and anomaly ozone profiles were binned into 5^{o} latitude bands (36 bands for 90^{o}S-90^{o}N, similar to MLS/GMI climatology) between 1 and 261 hPa (30 pressure levels).

The main challenge of EOF analysis is interpretation of derived EOFs and EOF time coefficients and their attribution to specific geophysical processes. As described in the Supplementary Materials, the construction of this REOF climatology required only total ozone and tropical stratospheric zonal wind time series to explain most of stratospheric ozone profiles variability

(total EOF variance). We used MLS ozone anomalies expressed as ozone partial pressure for the REOF analysis rather than ozone mixing ratio because it helped to attribute the REOF-1 time coefficient directly to total ozone column measurements at all latitudes. The first REOF vector with the MOD total ozone time series as a proxy explains about 50-70% of the inter-annual ozone variability. -Next, we derived a second REOF-2 that we attributed to the QBO and used the equatorial zonal wind time series as a proxy for REOF-2. The sum of these two REOFs explains about 70-80% of the inter-annual variability in de-seasonalized MLS zonal mean ozone profiles. Since only MLS profiles are used to constrain the vertical shapes of the REOFs and time coefficients are described by total ozone and zonal winds, this REOF climatology can be used in the future (even after MLS stops operating) or can be extended into the past to the pre-Aura time period whenever total column ozone and wind data are available.

The REOF climatology was finally converted from the ozone partial pressures defined at 30 MLS levels to volume mixing ratio (ppmv) and partial ozone column (DU km^{-1}) at the 1 km Z^* levels (defined in section 3.2) identical to the MLS/GMI climatology. The REOF climatological values at levels below ~9 km and above ~48 km are very small in contributing to inter-annual variability of ozone and are set to zero. Since the REOF climatology uses zonal wind and total ozone time series that can have long-term trends, we applied a very low frequency (VLF) digital low-pass filter to the final derived REOF climatology to remove long-term decadal variability. This was done to ensure that the climatology captures only inter-annual variability in monthly zonal mean ozone anomaly profiles without inducing decadal trends if used as a prior in ozone retrieval. The frequency response of the applied VLF digital filter (Stanford and Ziemke, 1993) is exactly 0.0 (1.0) at zero (Nyquist) frequency with an amplitude of 0.5 at frequency 0.00333 $month^{-1}$; the filter was also designed to have zero phase shift at all frequencies.

We demonstrate that the REOF climatology does very well in capturing inter-annual variability of monthly zonal-mean stratospheric ozone. The high vertical resolution of MLS ozone limb measurements of ~3 km resolves much of the vertical variability of ozone caused by low-frequency and episodic processes such as the QBO, extra-tropical stratospheric warmings, and other year-round planetary-scale wave events (e.g., Ziemke et al., 2014, and references therein). Many nadir instrument ozone profile retrievals have coarse vertical resolution of ~ 6 to 10 km or

greater (such as from SBUV or OMI) and cannot do nearly as well at resolving vertical changes in stratospheric ozone.

The magnitude of inter-annual variability in profile ozone, captured by the REOF climatology, is shown in Fig. 6 as calculated standard deviations in DU km^{-1} for the 1970-2018 period. In the tropical low latitudes from 10°S-10°N the main source of inter-annual variability is the QBO. However, larger inter-annual variability occurs in the SH extra-tropics due to the QBO and additional dynamical sources. In an effort to understand the contribution of non-QBO processes to the inter-annual variability we also generated a climatology using only equatorial QBO zonal winds as a proxy (see Fig. S4 in the Supplementary Material). When compared to the REOF climatology in Fig. 6, only a very small fraction of inter-annual variability is captured in the extra-tropics for the QBO-only climatology.

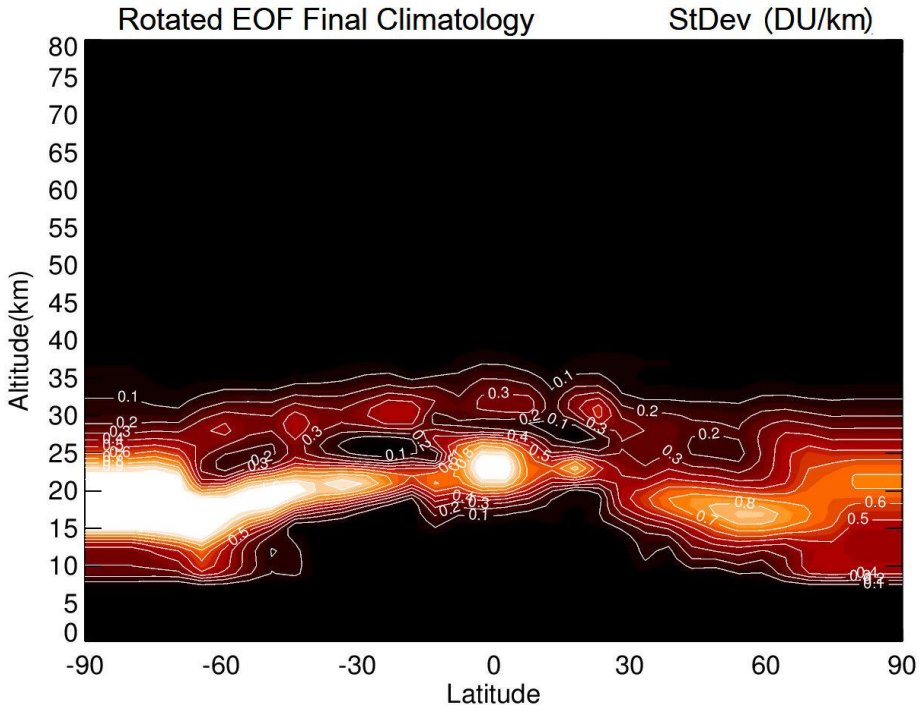

Figure 6. Temporal standard deviation (in DU km^{-1}) for 1970-2018 for the final REOF ozone climatology (i.e., Eq. (S10) in Supplementary Materials). The inter-annual variability in the tropical low latitudes is almost entirely due to the QBO. Inter-annual variability in the extra-tropics comes from the QBO coupled with other non-QBO related inter-annual variability.

The long record of the REOF inter-annual ozone profile climatology has been compared with de-seasonalized ozone profile measurements from SAGE II and Aura MLS for 1984-2018 (Fig. 7). The top panel in Fig. 7a shows comparisons of upper stratospheric column ozone anomalies (Z^*=25-50 km) between REOF (black curve) and SAGE (red asterisks) for years 1984-2005 in the tropics (10°S-10°N). The bottom panel in Fig. 7a shows a similar comparison between REOF and MLS for 2005-2018. Figure 7b is the same as in Fig. 7a, except for the lower stratosphere (Z^* =17-25 km).

The SAGE II sampling ozone columns in Fig. 7 is sparse, averaging ~2-3 days of measurements for a given month in the 10°S-10°N latitude band shown. This means that the monthly SAGE measurements in Fig. 7 are more representative of daily profiles rather than monthly means. Ozone profiles on a daily basis in the tropics are distorted by propagating tropical waves with periods of days to weeks such as Kelvin waves, equatorial Rossby waves, and mixed Rossby-gravity waves (e.g., Timmermans et al., 2005; Ziemke and Stanford, 1994). As a result, the upper and lower stratospheric columns in Fig. 7 for SAGE II will have noisy month-to-month variations of several DU because of these tropical waves. The Supplementary Material includes further discussion and figures for the REOF climatology.

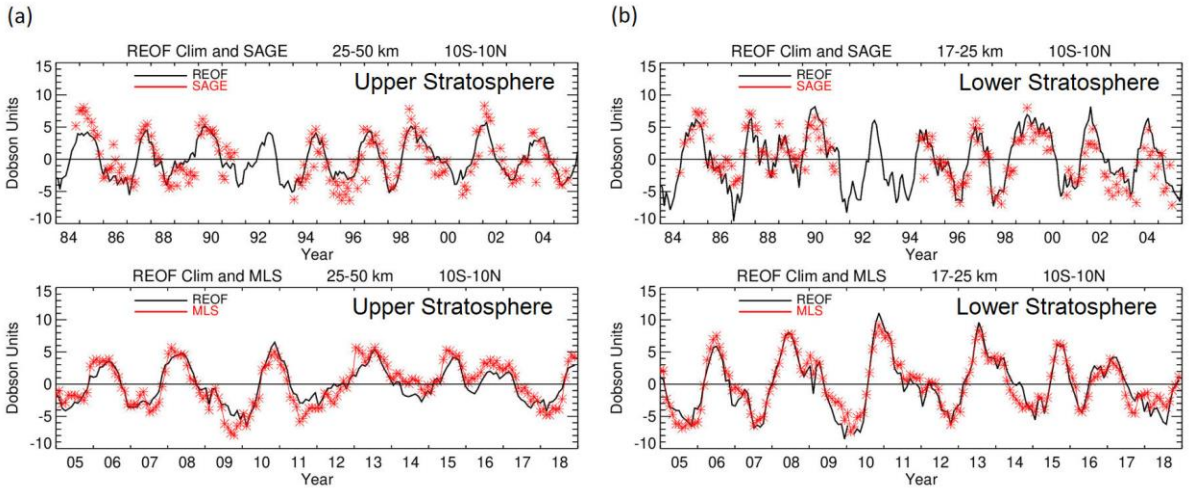

Figure 7. (a) Top panel is zonal-mean upper stratospheric column ozone (in Dobson Units) for the REOF climatology (black curve) and deseasonalized SAGE II (red asterisks) spanning 1984-

2005 and averaged between 10°S-10°N. The SAGE data are deseasonalized monthly zonal means. All column amounts are calculated by integrating ozone profiles for Z^*=25-50 km (~28 to 1 hPa). Bottom panel is the same as the top panel, but with MLS in place of SAGE and for the time period 2005-2018. (b) Same as (a), but for the lower stratosphere with Z^*=17-25 km (~88 to 28 hPa).

5. Summary.

We have produced a new MLS/GMI seasonal ozone profile climatology by combining ozone profiles from the M2GMI model simulation with MLS v4.2 measurements. M2GMI is used primarily for tropospheric ozone and MLS for stratospheric ozone, with the two ozone profile datasets blended together in the low stratosphere; the result is a merged zonal-mean, 12-month global ozone profile climatology at 5° latitude resolution with Z^* altitude range 0-80 km (1 km vertical sampling). Our main interest in generating the MLS/GMI climatology is to use it as a priori information in satellite ozone retrieval algorithms. However, it is also useful as a baseline for evaluating various modeled or measured ozone seasonal and inter-annual variability, and in studies involving corresponding ozone radiative forcing as inferred from atmospheric radiative transfer calculations.

In previous studies we generated several ozone profile climatologies based on combining ozonesondes with either SAGE or MLS satellite measurements (e.g., McPeters et al., 2007; McPeters and Labow, 2012; Labow et al., 2015). We have compared the new MLS/GMI climatology in detail with the ML climatology of McPeters and Labow (2012) that used ozonesondes for tropospheric ozone profiles. The M2GMI model simulation provides an improved ozone climatology for the troposphere compared to the ML climatology due to having much better spatial and temporal coverage than the sondes.

We also developed a time-dependent climatology of monthly zonal-mean profile ozone anomalies representing inter-annual variability. This inter-annual climatology was constructed using a rotational EOF analysis of Aura MLS monthly zonal-mean profile ozone anomalies from August 2004 – December 2016 within each 5° latitude band. The analysis shows that the first

two leading EOFs explain ~70-80% of inter-annual variability of profile ozone at all latitudes. Furthermore, total ozone and tropical zonal wind time series correlate well with the two leading EOF coefficient time series and were used as proxies to extend information outside the Aura MLS time range. We used these relationships to reconstruct anomalies at 5^o latitudinal resolution for $Z^* = 0$-80 km and 1970-2018. This REOF time-dependent climatology was compared to a similar climatology based on only tropical QBO winds. The advantage of the REOF climatology is that allows for a much more thorough representation of inter-annual variability of stratospheric ozone than just the QBO.

The REOF time-dependent climatology of ozone profile anomalies can be easily added to the MLS/GMI seasonal climatology to simulate seasonal+inter-annual variability of stratospheric ozone. We note that both the MLS/GMI 12-month climatology and REOF climatology were generated using Aura time period MLS ozone measurements and neither of them account for long-term trends in stratospheric ozone.

Acknowledgments. We thank the NASA Jet Propulsion Laboratory MLS team for the MLS v4.2 ozone dataset and the SHADOZ, WOUDC and NDACC personnel for providing the extensive ozonesonde measurements that we used for our study. We also thank the NASA MAP program for supporting the MERRA-2 GMI simulation and the NASA Center for Climate Simulation (NCCS) for providing high-performance computing resources. Special thanks go to the NASA GMI group especially Sarah Strode regarding the MERRA-2 GMI simulation. Funding for this research was provided in part by NASA NNH14ZDA001N-DSCOVR.

Data availability. Data description for MLS v4.2 ozone and links to the data can be obtained from websites https://mls.jpl.nasa.gov/products/o3_product.php (last access 16 April 2021) and https://disc.gsfc.nasa.gov/ (last access 16 April 2021). MERRA-2 GMI model description and access is available at https://acd-ext.gsfc.nasa.gov/Projects/GEOSCCM/MERRA2GMI/ (last access: 16 April 2021). The MOD total ozone measurements are available from the webpage https://acd-ext.gsfc.nasa.gov/Data_services/merged/. Tropical QBO winds were provided by the

University of Berlin from https://www.geo.fu-berlin.de/met/ag/strat/produkte/qbo/qbo.dat. The seasonal and inter-annual climatology products derived from our study are available for the general public using direct links from the NASA webpage https://avdc.gsfc.nasa.gov/.

References.

Bass, A. M., and R. J. Paur, The ultraviolet cross-sections of ozone, I: The measurements, in *Proc. Quad. Ozone Symp.*, edited by C. Zerefos, and A. Ghazi, pp. 606–616, Reidel, Dordecht, Halkidiki, Greece, 1984.

Bourgeois, I., J. Peischl, C. R. Thompson, K. C. Aikin, T. Campos, H. Clark, R. Commane, B. Daube, G. W. Diskin, J. W. Elkins, R.-S. Gao, A. Gaudel, E. J. Hintsa, B. J. Johnson, R. Kivi, K. McKain, F. L. Moore, D. D. Parrish, R. Querel, E. Ray, R. Sánchez, C. Sweeney, D. W. Tarasick, A. M. Thompson,V. Thouret, J. C. Witte, S. C. Wofsy, and T. B. Ryerson, Global-scale distribution of ozone in the remote troposphere from the ATom and HIPPO airborne field missions Atmos. Chem. Phys., 20, 10611–10635, https://doi.org/10.5194/acp-20-10611-2020, 2020.

Duncan, B. N., R. V. Martin, A. C. Staudt, R. Yevich, and J. A. Logan, Interannual and seasonal variability of biomass burning emissions constrained by satellite observations, *J. Geophys. Res. Atmos., 108*(D2), doi:10.1029/2002jd002378, 2003.

Duncan, B.N., S.E. Strahan, Y. Yoshida, S.D. Steenrod, and N. Livesey, Model study of cross-tropopause transport of biomass burning pollution, *Atmos. Chem. Phys., 7*, 3713-3736, doi:10.5194/acp-7-3713-2007, 2007.

Fishman, J., C. E. Watson, J. C. Larsen, and J. A. Logan, Distribution of tropospheric ozone determined from satellite data, *J. Geophys. Res., 95*(D4), 3599-3617, 1990.

554 Frith, S. M., N. A. Kramarova, R. S. Stolarski, R. D. McPeters, P. K. Bhartia, and G. J. Labow,
555 Recent changes in total column ozone based on the SBUV Version 8.6 Merged Ozone Data Set,
556 *J. Geophys. Res. Atmos.,119*, 9735–9751, doi:10.1002/2014JD021889, 2014.
557
558 Frith, S. M., P. K. Bhartia, L. D. Oman, N. A. Kramarova, R. D. McPeters, and G. J. Labow,
559 Model-based climatology of diurnal variability in stratospheric ozone as a data analysis tool
560 *Atmos. Meas. Tech.*, *13*, 2733–2749, https://doi.org/10.5194/amt-13-2733-2020, 2020.
561
562 Froidevaux, L., et al., Validation of Aura Microwave Limb Sounder stratospheric ozone
563 measurements, *J. Geophys. Res.*, 113, D15S20, doi:10.1029/2007JD008771, 2008.
564
565 Gelaro, R., W. McCarty, M.J. Suárez, R. Todling, A. Molod, L. Takacs, C.A. Randles, A.
566 Darmenov, M.G. Bosilovich, R. Reichle, K. Wargan, L. Coy, R. Cullather, C. Draper, S. Akella,
567 V. Buchard, A. Conaty, A.M. da Silva, W. Gu, G. Kim, R. Koster, R. Lucchesi, D. Merkova, J.E.
568 Nielsen, G. Partyka, S. Pawson, W. Putman, M. Rienecker, S.D. Schubert, M. Sienkiewicz, and
569 B. Zhao, The Modern-Era Retrospective Analysis for Research and Applications, Version 2
570 (MERRA-2), *J. Climate*, *30*, 5419–5454, https://doi.org/10.1175/JCLI-D-16-0758.1, 2017.
571
572 Giglio, L., J. Randerson, and G. van der Werf, Analysis of daily, monthly, and annual burned
573 area using the fourth-generation global fire emissions database (GFED4), *J. Geophys. Res.*
574 *Bio.Sci.*, *118*(1), 317-328, doi:10.1002/jgrg.20042, 2013.
575
576 Granier, C., B. Bessagnet, T. Bond, A. D'Angiola, H. D. van der Gon, et al., Evolution of
577 anthropogenic and biomass burning emissions of air pollutants at global and regional scales
578 during the 1980–2010 period. *Climatic Change*, *109*, 163–190, doi:10.1007/s10584-011-0154-1,
579 2011.
580
581 Jaeglé, L., V. Shah, J. A. Thornton, F. D. Lopez-Hilfiker, B. H. Lee, E. E. McDuffie, et al.,
582 Nitrogen oxides emissions, chemistry, deposition, and export over the Northeast United States
583 during the WINTER aircraft campaign, J. Geophys. Res. Atmos., 123, 12,368–12,393,
584 https://doi.org/10.1029/2018JD029133/, 2018.

Jiang, Y. B., et al., Validation of Aura Microwave Limb Sounder Ozone by ozonesonde and lidar measurements, *J. Geophys. Res.*, 112, D24S34, doi:10.1029/2007JD008776, 2007.

Kutzbach, J. E., Empirical eigenvectors of sea-level pressure, surface temperature and precipitation complexes over North America, *J. App. Meteorol., 6*, 791-802, https://doi.org/10.1175/1520-0450(1967)006<0791:EEOSLP>2.0.CO;2, 1967.

Labow, G. J., J. R. Ziemke, R. D. McPeters, D. P. Haffner, and P. K. Bhartia, A total ozone-dependent ozone profile climatology based on ozonesondes and Aura MLS data, *J. Geophys. Res. Atmos., 120*, 2537-2545, doi:10.1002/2014JD022634, 2015.

Lamarque, J.-F., T. C. Bond, V. Eyring, C. Granier, A. Heil, Z. Klimont, D. Lee, C. Liousse, A. Mieville, B. Owen, M. G. Schultz, D. Shindell, S. J. Smith, E. Stehfest, J. Van Aardenne, O. R. Cooper, M. Kainuma, N. Mahowald, J. R. McConnell, V. Naik, K. Riahi, and D. P. van Vuuren, Historical (1850-2000) gridded anthropogenic and biomass burning emissions of reactive gases and aerosols: methodology and application, *Atmos. Chem. Phys., 10*(15), 7017-7039, doi:10.5194/acp-10-7017-2010, 2010.

Livesey, N. J., Read, W. G., Froidevaux, L., Lambert, A., Manney, G. L., Pumphrey, H. C., Santee, M. L., Schwartz, M. J., Wang, S., Cofield, R. E., Cuddy, D. T., Fuller, R. A., Jarnot, R. F., Jiang, J. H., Knosp, B. W., Stek, P. C., Wagner, P. A., and Wu, D. L.: *EOS MLS Version 3.3 Level 2 data quality and description document, Tech. rep., Jet Propulsion Laboratory*, available at: http://mls.jpl.nasa.gov/), 2011.

McPeters, R. D., G. J. Labow, and J. A. Logan, Ozone climatological profiles for satellite retrieval algorithms, *J. Geophys. Res., 112*, D05308, doi:10.1029/2005JD006823, 2007.

McPeters, R. D., and G. J. Labow, Climatology 2012: An MLS and sonde derived ozone climatology for satellite retrieval algorithms, *J. Geophys. Res., 117*, doi:10.1029/2011JD017006, 2012.

McPeters, R. D., P. K. Bhartia, D. Haffner, G. J. Labow, and L. Flynn, The version 8.6 SBUV ozone data record: An overview, *J. Geophys. Res., 118*, 8032–8039, doi:10.1002/jgrd.50597, 2013.

Molod, A., L. Takacs, M. Suarez, and J. Bacmeister, Development of the GEOS-5 atmospheric general circulation model: evolution from MERRA to MERRA2, *Geosci. Mod. Dev., 8*, doi:10.5194/gmd-8-1339-2015, 2015.

Oman, L. D., A. R. Douglass, J. R. Ziemke, J. M. Rodriguez, D. W. Waugh, and J. E. Nielsen, The ozone response to ENSO in Aura satellite measurements and a chemistry-climate simulation, *J. Geophys. Res., 118*, 965-976, doi:10.1029/2012JD018546, 2013.

Orbe, C., L. D. Oman, S. E. Strahan, D. W. Waugh, S. Pawson, L. L. Takacs, and A. M. Molod, Large-Scale Atmospheric Transport in GEOS Replay Simulations, *J. Adv. Mod. Earth Sys., 9*, 2545-2560, 2017.

Park, J. H., M. K. Ko, C. H. Jackman, R. A. Plumb, J. A. Kaye, and K. H. Sage, Models and Measurements Intercomparison II, *NASA Tech. Memo., NASA/TM-1999–209554, 502 pp*., 1999.

Parrish, A., Boyd, I. S., Nedoluha, G. E., Bhartia, P. K., Frith, S. M.,Kramarova, N. A., Connor, B. J., Bodeker, G. E., Froidevaux,L., Shiotani, M., and Sakazaki, T.: Diurnal variations of strato-spheric ozone measured by ground-based microwave remotesensing at the Mauna Loa NDACC site: measurement validationand GEOSCCM model comparison, Atmos. Chem. Phys., 14,7255–7272, https://doi.org/10.5194/acp-14-7255-2014, 2014.

Richman, M. B., Rotation of principal components, *J. Clim., 6*, 293-335, https://doi.org/10.1002/joc.3370060305, 1986.

Rodgers, C. D., Inverse methods for atmospheric sounding: theory and practice, *World Scientific Pupblishing Co., pp. 238,* London, United Kingdom, 2000.

Shepherd, T. G., D. A. Plummer, J. F. Scinocca, M. I. Hegglin, V. E. Fioletov, M. C. Reader, E. Remsberg, T. von Clarmann, and H. J. Wang, Reconciliation of halogen-induced ozone loss with the total-column ozone record, *Nature Geosci., 7*, doi:10.1038/NGEO2155, 2014.

Stanford, J. L., J. R. Ziemke, and S. Y. Gao, Stratospheric circulation features deduced from SAMS constituent data, *J. Atmos. Sci., 50*, 226-246, 1993.

Stauffer, R. M., A. M. Thompson, L.D. Oman, and S.E. Strahan, The effects of a 1998 observing system change on MERRA-2-based ozone profile simulations. *J. Geophys. Res. Atmos., 124*, 7429-7441, https://doi.org/10.1029/2019JD030257, 2019.

Strode, S. A., J. M. Rodriguez, J. A. Logan, O. R. Cooper, J. C. Witte, L. N. Lamsal, M. Damon, B. Van Aartsen, S. D. Steenrod, and S. E. Strahan, Trends and variability in surface ozone over the United States, *J. Geophys. Res. Atmos., 120*(17), 9020-9042, doi:10.1002/2014JD022784, 2015.

Strode, S. A., J. S. Wang, M. Manyin, B. N. Duncan, R. Hossain, C. A. Keller, S. E. Michel, and J. W. C. White, Strong sensitivity of the isotopic composition of methane to the plausible range of tropospheric chlorine, Atmos. Chem. Phys., 20, 8405–8419, https://doi.org/10.5194/acp-20-8405-2020, 2020.

Thompson, A. M., Witte, J. C., Sterling, C., Jordan, A., Johnson, B. J., Oltmans, S. J., Fujiwara, M., Vömel, H., Allaart, M., Piters, A., Coetzee, G. J. R., Posny, F., Corrales, E., Andres Diaz, J., Félix, C., Komala, N., Lai, N., Maata, M., Mani, F., Zainal, Z., Ogino, S.-Y., Paredes, F., Luiz Bezerra Penha, T., Raimundo da Silva, F., Sallons-Mitro, S., Selkirk, H. B., Schmidlin, F. J., Stuebi, R., and Thiongo, K.: First reprocessing of Southern Hemisphere Additional Ozonesondes

(SHADOZ) Ozone Profiles (1998–2016). 2. Comparisons with satellites and ground-based instruments, *J. Geophys. Res., 122*, 13000–13025, https://doi.org/10.1002/2017JD027406, 2017.

Timmermans, R. M. A., R. F. van Oss, and H. M. Kelder, Equatorial Kelvin wave signatures in ozone profile measurements from Global Ozone Monitoring Experiment (GOME), *J. Geophys. Res., 110*, D21103, doi:10.1029/2005JD005929, 2005.

Wallace, J. M., R. L. Panetta, and J. Estberg, Representation of the equatorial stratospheric Quasi-Biennial Oscillation in EOF phase space, *J. Atmos. Sci., 50*, 12, 1751-1762, doi:10.1175/1520-0469(1993)050<1751:ROTESQ>2.0.CO;2, 1993.

Wargan, K., C. Orbe, S. Pawson, J. R. Ziemke, L. D. Oman, M. A. Olsen, et al., Recent decline in extratropical lower stratospheric ozone attributed to circulation changes. *Geophys. Res. Lett., 45*, 5166–5176. https:// doi.org/10.1029/2018GL077406, 2018.

Witte, J. C., Thompson, A. M., Smit, H. G. J., Fujiwara, M., Posny, F., Coetzee, G. J. R., Northam, E. T., Johnson, B. J., Sterling, C. W., Mohammed, M., Ogino, S.-Y., Jordan, A., daSilva, F. R., and Zainal, Z.: First reprocessing of Southern Hemisphere Additional OZonesondes (SHADOZ) profile records (1998–2015) 1: Methodology and evaluation, *J. Geophys. Res., 122*, 6611–6636, https://doi.org/10.1002/2016JD026403, 2017.

Ziemke, J. R., and J. L. Stanford, Quasi-biennial oscillation and tropical waves in total ozone, *J. Geophys. Res., 99*, 23,041-23,056, 1994.

Ziemke, J. R., S. Chandra, A. Thompson, and D. McNamara, Zonal asymmetries in Southern Hemisphere column ozone: Implications of biomass burning, *J. Geophys. Res., 101*, 14,421-14,427, doi:10.1029/96JD01057, 1996.

Ziemke, J. R., S. Chandra, G. J. Labow, P. K. Bhartia, L. Froidevaux, and J. C. Witte, A global climatology of tropospheric and stratospheric ozone derived from Aura OMI and MLS measurements, *Atmos. Chem. Phys., 11*, 9237-9251, doi:10.5194/acp-11-9237-2011, 2011.

Ziemke, J. R., M. A. Olsen, J. C. Witte, A. R. Douglass, S. E. Strahan, K. Wargan, X. Liu, M. R. Schoeberl, K Yang, T. B. Kaplan, S. Pawson, B. N. Duncan, P. A. Newman, P. K. Bhartia, M. K. Heney, Assessment and applications of NASA ozone data products derived from Aura OMI/MLS satellite measurements in context of the GMI Chemical Transport Model, *J. Geophys. Res. Atmos.*, *119*, 5671-5699,doi:10.1002/2013JD020914, 2014.